Journal of Ceramic Processing Research. Vol. 24, No. 5, pp. 894~898 (2023)
(Received 15 August 2023, Received in revised form 10 October 2023, Accepted 15 October 2023)
https://doi.org/10.36410/jcpr.2023.24.5.894

J O U R N A L O F
Ceramic Processing Research

Structural, magnetic properties of nickel-substituted strontium W-type ferrites

Jinsong Li, Xiubin Zhao and Ailin Xia*
School of Materials Science and Engineering, Anhui University of Technology, Maanshan 243002, China

Nickel substituted W-type strontium ferrites $Sr_{0.9}Ce_{0.1}Zn_{2-x}Ni_xFe_{16}O_{27}$ (x=0.0, 0.2, 0.4, 0.6, 0.8 and 1.0) were prepared by a ceramic method. The specimens exhibited a single-phase W-type structure when the Ni content (x) is $0 \le x \le 1$. With the increasing content of nickel dopant, the particles exhibited a hexagonal plate-like shape. The saturation magnetization and remanent magnetization increased x from 0.0 to 0.6, then decreased with $x > 0.6$. The coercivity of specimens increased gradually for $x \le 0.2$ and then began to decrease from $x = 0.3$; the coercivity shows a downward trend with the Ni content continuing to increase. Subsequently, as the Ni content increases, there is a downward trend compared to the unsubstituted specimens.

Keywords: W-type ferrite, Ceramic method, Structure, Magnetic properties.

Introduction

As a crucial functional material, magnetic ferrites can be divided into three categories: spinel, garnet and magneto plumbite-type. According to the different characteristics of crystal structure, the magneto plumbite-type ferrites are further divided into six types: M, W, X, Y, Z and U [1-3]. The W-type ferrites have both complex magnetic properties and high-frequency soft magnetic characteristics. Due to the high saturation magnetization (M_s) and the excellent chemical stability, W-type ferrites are used in microwave equipment and electromagnetic wave absorbers [4]. The chemical composition formula of W-type ferrites is $AMe_2Fe_{16}O_{27}$. W-type ferrites belong to the hexagonal crystal system. The unit cell is composed of SSRS*S*R* stacking sequences, which can also be seen as the stacking of M-type "SR blocks" and spinel "S blocks" or the addition of an "S blocks" between two "R blocks" in the M-type structure. The iron ions can be located in seven different lattice positions [4, 5].

Different preparation methods for Sr ferrites have been proposed, such as the sol-gel [6, 7], chemical co-precipitation [8], ceramic method [9], and glass crystallization technique [10]. In the study of W-type ferrites, the ceramic method is widely used to achieve mass production due to their simple manufacturing process, stoichiometric composition, controllable grain size, rich raw materials and low price.

Theoretically, the M_s of W-type ferrite is about 10% higher than that of M-type ferrite, while their anisotropic magnetic field is almost the same. Moreover, the W-type ferrite has two kinds of cationic crystal sites, which can be replaced by the various bivalent or trivalent cations, which can tailor the magnetism in a broader range compared with M-type ferrite [11, 12]. Tang et al. [9] prepared $BaCo_xFe_{2-x}$ W-type ferrites by a ceramic method. It was found that the magnetic anisotropy field of specimens decreased with the increase of Co content. Akhter et al. [13] used a sol-gel auto combustion method to synthesize $CaPb_{2-x}Yb_xFe_{16}O_{27}$ W-type ferrites. They found that the AC conductivity and the natural/imaginary parts of the dielectric constant exhibited an increasing and a decreasing behavior with the increase of dopant content, respectively. The microstructure and magnetic properties of Mg-Cu substituted $BaMg_{2-x}Cu_xFe_{16}O_{27}$ prepared by the ceramics process have been discussed by Niu et al. [14]. The lattice constant increased with the increase of Cu content (x), while the lattice constant c decreased. Ghasemi [15] reported highly magnetized $SrCo_{2-x}Mn_xFe_{16}O_{27}$ (x = 0-0.5) W-type ferrites prepared by a coprecipitation route. The magnetization reversal mechanism of the specimen followed the Stoner Wohlfarth mechanism, and the domain wall motion mechanism was also discussed.

However, the effect of nickel substitution on the magnetic properties of strontium W-type ferrite synthesized by the ceramic method was still not reported. Therefore, in this study, the W-type ferrite $Sr_{0.9}Ce_{0.1}Zn_{2-x}Ni_xFe_{16}O_{27}$ (x is from 0.0 to 1.0 with the steps of 0.2.) magnetic powders were prepared by ceramic method, and the effects of the nickel content (x) on the structure and the magnetic properties of W-type ferrites $Sr_{0.9}Ce_{0.1}Zn_{2-x}Ni_xFe_{16}O_{27}$ are systematically studied.

*Corresponding author:
Tel : +86-0555-2322181
Fax: +86-0555-2311570
E-mail: alxia@126.com

Experimental Procedures

Materials

The starting materials of Fe_2O_3 (99.2% purity), $SrCO_3$ (98% purity), CeO_2 (99% purity), ZnO (99% purity) and NiO (99% purity) powders were used without further purification in this study.

Preparation of W-type ferrites $Sr_{0.9}Ce_{0.1}Zn_{2-x}Ni_xFe_{16}O_{27}$ powders

150 g specimens with the nominal composition of $Sr_{0.9}Ce_{0.1}Zn_{2-x}Ni_xFe_{16}O_{27}$ (x is from 0.0 to 1.0 with 0.2 steps) were obtained via a conventional ceramic method. Then, the mixed powders were ball-milled with steel balls of a diameter of 6 mm for 4 hours, using water as the disperser. The slurry obtained was dried and pressed into some small pieces, and then calcined at 1300 °C in a muffle furnace for 2 hours in the air atmosphere. Afterwards, the calcined pieces were crushed by a vibrator to prepare specimen powders through a 100-mesh sieve.

Characterization

The phase composition of specimens was obtained by an X-ray diffractometer (XRD, PANalytical X'Pert Pro) using Cu Kα (λ=1.5406 Å) radiation. The scanning range is between 20° and 80° with the steps of 0.01°. A field emission scanning electron microscope (FESEM, HITACHI S-4800) was used to measure the morphologies of specimens. A vibrating sample magnetometer (VSM, MicroSense EZ7) was used to measure the RT magnetic properties at a maximum external field of 20,000 Oe.

Results and Discussion

Structure and morphology

Fig. 1 shows the XRD patterns of obtained specimens. Compared with all the peaks in the standard JCPDS card XRD patterns (PDF#00-052-1860), no other impurity peaks were found in Fig. 1, indicating the single phase W-type structures in all the specimens. From Fig. 1, it can be seen that Ni^{2+} ions entered into the lattice without forming any other phase.

The lattice parameters a and c can be calculated from the values of d_{hkl} corresponding to (116) and (1010)

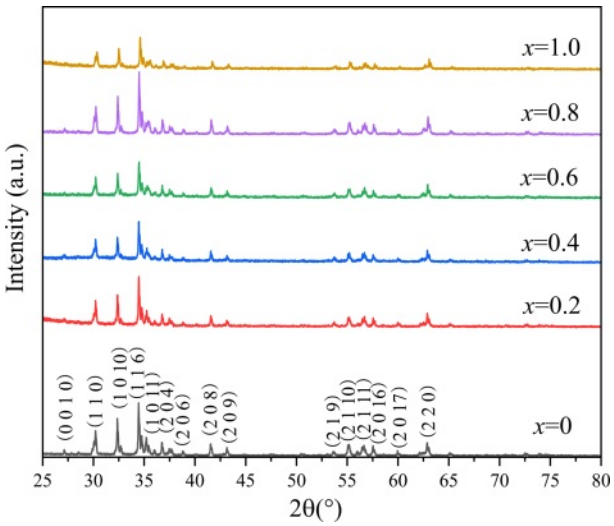

Fig. 1. XRD patterns of obtained W-type $Sr_{0.9}Ce_{0.1}Zn_{2-x}Ni_xFe_{16}O_{27}$ ferrites.

peaks and the following equations (1) and (2) [16, 17]:

$$d_{hkl} = \left(\frac{4}{3}\cdot\frac{h^2+hk+k^2}{a^2}+\frac{l^2}{c^2}\right)^{-1/2} \quad (1)$$

$$V_{\text{cell}} = a^2 c \sin 120° \quad (2)$$

where a and c are lattice constants; h, k and l are the Miller indices. d_{hkl} and V_{cell} are the crystal face spacing and the cell volume, respectively. The following equations (3) and (4) were used to calculate the X-ray density ($d_{X\text{-}ray}$) and the average crystallite size (D) [18, 19], respectively.

$$d_{X-\text{ray}} = \frac{2M}{N_A V_{\text{cell}}} \quad (3)$$

$$D = \frac{K\lambda}{\beta\cos\theta} \quad (4)$$

where N_A, K and λ are 6.02×10^{23}, 0.89 and 1.5406 Å, respectively; M, β and θ are the molar mass, the full-width at half-maximum and the Bragg's diffraction angle, respectively. The values calculated by the above formulas are listed in Table 1.

Fig. 2 shows the dependency of lattice constants a and c on x. It can be seen that with an increase of x from 0.0 to 1.0, both the lattice constants a and c show a decreasing trend. The lattice parameter a changes

Table 1. Different crystalline parameters calculated for specimens.

Ni(x)	a (Å)	c (Å)	c/a	$d_{X\text{-ray}}$ (g/cm^3)	V_{cel}(Å^3)	D(nm)
0	5.9096	32.8413	5.5573	5.181	993.2405	54.48
0.2	5.9062	32.8243	5.5576	5.1825	991.5844	58.34
0.4	5.9053	32.8172	5.5572	5.2001	991.0678	56.34
0.6	5.9032	32.8031	5.5568	5.1832	989.9375	50.47
0.8	5.9007	32.7966	5.5581	5.1852	988.9032	60.49
1.0	5.9004	32.7961	5.5583	5.2149	988.7876	55.23

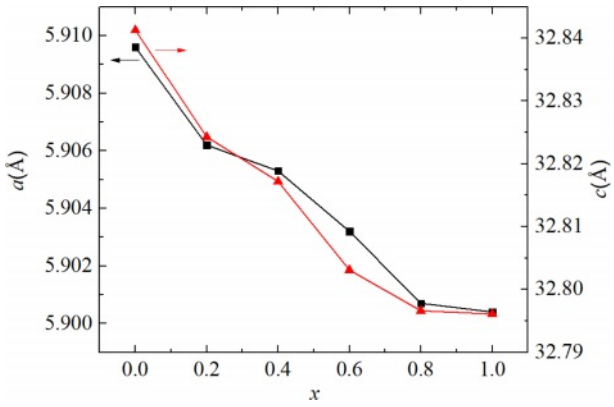

Fig. 2. The change of lattice constants *a* and *c* of specimens with different *x* from 0.0 to 1.0.

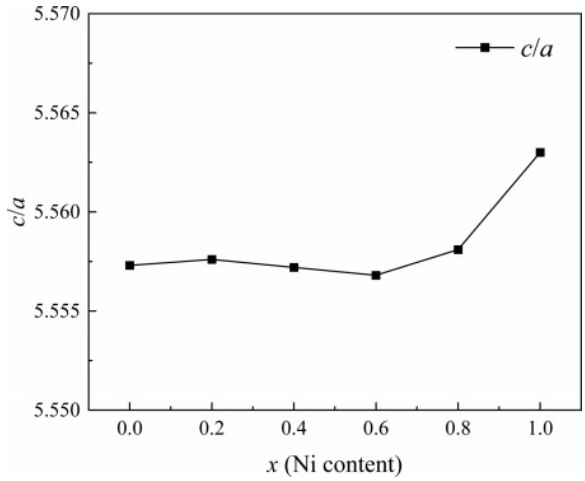

Fig. 3. The change *c*/*a* of specimens with different *x* from 0.0 to 1.0.

slightly, while the lattice parameter *c* decreases obviously from 32.8413 Å (*x*=0.00) to 32.7961 Å (*x*=1.0). The change of lattice parameters caused by ion substitution has also been reported in early literature [20-25]. It is well-known that the ionic radii of Zn^{2+} and Ni^{2+} are 0.82 and 0.78 Å, respectively [26]. As a result, after replacing Zn^{2+} with Ni^{2+}, the lattice parameters *a* and *c* become smaller in the specimens. Therefore, lattice deformation was caused by the Ni^{2+} substitution. In this study, with the increasing amount of Ni substitution, the lattice parameters decreased, resulting in a decrease of d_{hkl}, which exhibits the similar change of V_{cel} as listed in Table 1.

In W-type hexagonal ferrite, the *c*-axis rotates easily along the direction perpendicular to the hexagonal plane [27]. Thus rotation causes the change of *c* more quickly compared with *a*. The *c*/*a* ratio parameter is often used to detect structural types. Fig. 3 gives the change of lattice constants *a* and *c* in specimens with different *x* from 0.0 to 1.0. For W-type hexagonal structures, it can be considered that the *c*/*a* should be less than 5.585, as reported by Wagner in reference

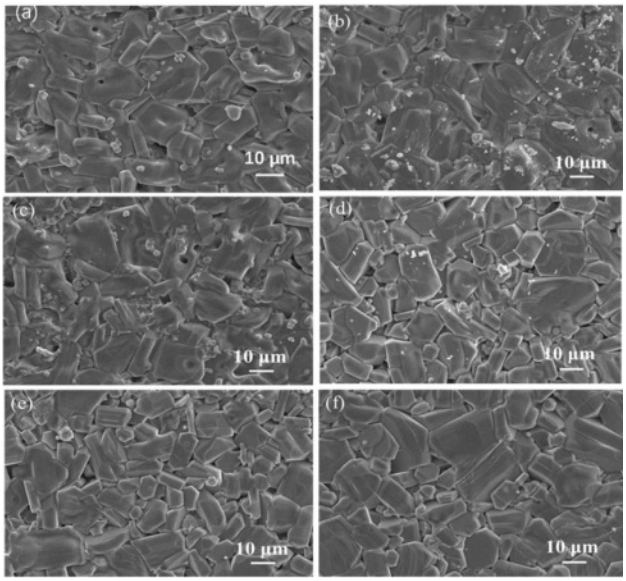

Fig. 4. Typical FE-SEM images of $Sr_{0.9}Ce_{0.1}Zn_{2-x}Ni_xFe_{16}O_{27}$ specimens with different *x*. (a-f): *x* is from 0.0 to 1.0 with steps of 0.2, respectively.

[28]. The ratios of *c*/*a* for all the specimens are listed in Table 1. In this study, the ratio of *c*/*a* was between 5.5568 and 5.5630, which remains stable with *x*.

Fig. 4 gives the typical FE-SEM images of specimens with different *x*. Some typical hexagonal grains can be observed in the images, and the particle morphology is clear. The comparison between the replaced specimens and the unsubstituted specimens showed that different *x* had no significant effect on the morphology of the grains.

Magnetic properties

Fig. 5 shows the RT magnetic hysteresis loops of $Sr_{0.9}Ce_{0.1}Zn_{2-x}Ni_xFe_{16}O_{27}$ specimens. The corresponding magnetic properties of specimens with different *x*, including the saturation magnetization (M_s), the

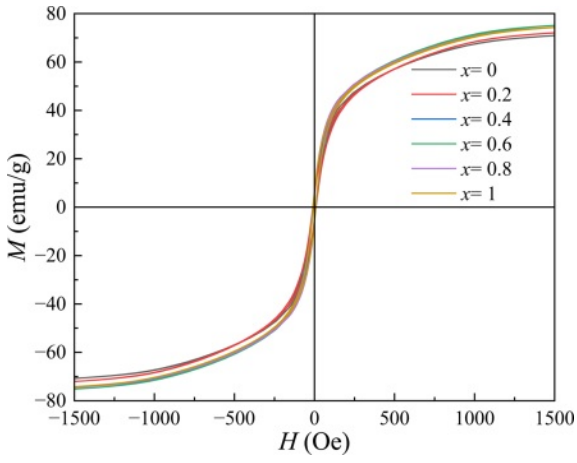

Fig. 5. RT magnetic hysteresis loops of $Sr_{0.9}Ce_{0.1}Zn_{2-x}Ni_xFe_{16}O_{27}$ specimens with different *x*.

Table 2. Magnetic properties of specimens with different *x*.

Ni(*x*)	M_s(emu/g)	M_r(emu/g)	M_r/M_s	H_c(Oe)
0	71.800	5.963	0.083	123.2
0.2	72.393	5.972	0.083	124.2
0.4	74.735	6.062	0.081	110.7
0.6	75.486	6.071	0.080	105.8
0.8	74.757	5.963	0.080	99.3
1.0	74.633	5.881	0.079	102.0

remanent magnetization (M_r), the coercivity (H_c) and the square ratio (M_r/M_s), were listed in Table 2. It should be pointed out that in Fig. 5, the values of M at the magnetic field of 20 kOe were reckoned as the M_s.

In this study, as can be observed from Table 2 and Fig. 6, the M_s and M_r of specimens first increase from 71.800 and 5.963 emu/g (x=0.0) to 75.486 and 6.071 emu/g (x=0.6), respectively, while both gradually decrease for $x \geq 0.6$. The H_c of specimens exhibits the same tendency as M_s and M_r. The trends of M_s, M_r and H_c are consistent with the previous studies [29-32].

In Zn_2W hexagonal ferrite, it has been reported that the magnetic moment of Zn^{2+} ions is 0.0 μ_B, Zn^{2+} and Ni^{2+} ions preferentially occupy the tetrahedral (4*e* and 4f_{IV}) and the octahedral (4f_{VI} and 6g) sites [24, 26, 33], respectively. Moreover, Ni^{2+} has a higher octahedral position preference energy than Fe^{3+}. Therefore, Fe^{3+} cations prefer to occupy tetrahedral positions [5]. When Ni^{2+} ions replace Zn^{2+} ions in the W-type structure, the superexchange position between the tetrahedral and octahedral positions is strengthened, increasing the total magnetic moment. Therefore, the M_s of Ni-substituted W-type hexaferrites increases gradually. Meanwhile, as the content of Zn ions decreases, the nonmagnetic of Zn^{2+} ions occupying the octahedral sites replace the tetrahedral ones and transfer to the octahedral sites in the S blocks. Fe^{3+} ions migrate from the

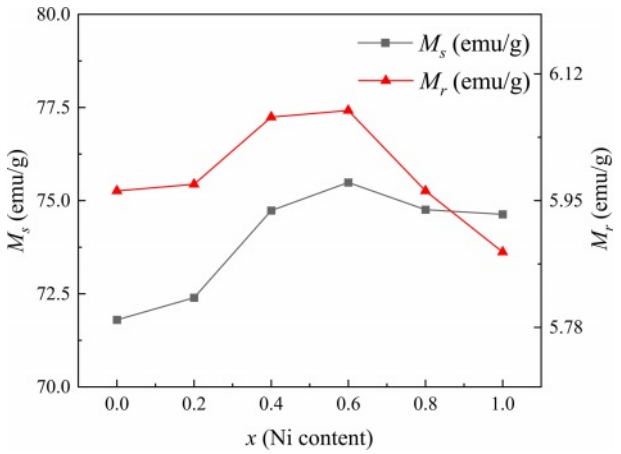

Fig. 6. Saturation magnetization (M_s), remanent magnetization (M_r) of specimens with different nickel content (x) from 0 to 1.0.

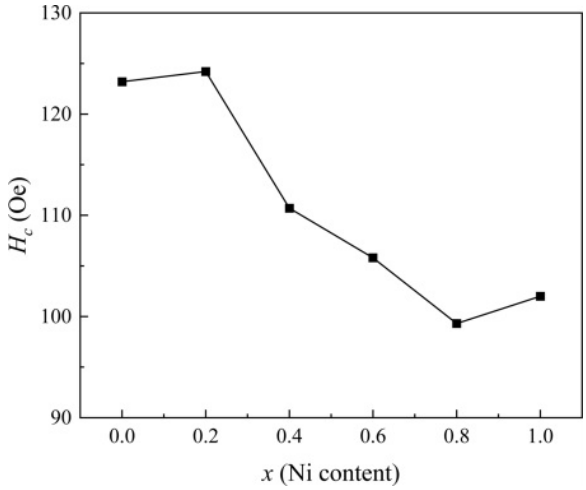

Fig. 7. The H_c of specimens with different x from 0.0 to 1.0.

octahedral to the tetrahedral sites in S blocks, thus affecting the position of Fe^{3+} ions in the lattice and causing a certain tilt in the magnetic moment direction of Fe^{3+} ions [5]. In addition, since the magnetic moment of Ni^{2+} ions (2.0 μ_B) is smaller than that of Fe^{3+}ions (5.0 μ_B) [5], the superexchange will be weakened when the substitution of Ni^{2+} ions reaches a certain extent, which consequently reduces the M_s. This well explains the decreasing M_s and M_r for the specimens with $x \geq 0.6$.

From Fig. 7 and Table 2, it can be observed that the H_c decreases for x between 0.2 and 0.8. Generally, the grain size dominates the value of H_c for magnetic materials. Previous investigation [34] has reported that the changes of grain size can enhance or reduce H_c. Usually, the H_c is inversely proportional to the increasing grain size higher than the critical size of the single domain (D_c) in the sintered specimens [35]. However, it is also affected by the crystallite shape, stress, lattice defects and so on. Therefore, in this study, it can be seen from the figure that the H_c changes irregularly with the increasing x. Overall, compared with specimens without Ni (x=0.0), the H_c of specimens with x>0.0 shows a downward trend.

Conclusions

Nickel substituted W-type strontium ferrites with the nominal composition of $Sr_{0.9}Ce_{0.1}Zn_{2-x}Ni_xFe_{16}O_{27}$ (x is from 0.0 to 1.0 with the steps of 0.2.) were obtained by the traditional ceramic method. It was found that a pure W-phase hexagonal crystal structure without any other impurity was obtained for all the specimens. With the increasing x, the lattice parameters a and c decreased obviously, while the c/a ratio changed slightly. The M_s and M_r of specimens increased for x from 0 to 0.6 and then decrease for x higher than 0.6. However, the H_c changes irregularly with the increasing x due to the different dominating mechanisms.

References

1. N.A. Majid and A.K. Muhammad, Ceram. Int. 44 (2018) 12921-12928.
2. S. Zhang, C.X. Cao, S.B. Su, A.L. Xia, H.Y. Zhang, H.L. Li, Z.Y. Liu, and C.G. Jin, J. Adv. Ceram. 12.4 (2023) 815-821.
3. Y.J. Yang, X.S. Liu, and S.J. Feng, J. Ceram. Process. Res. 21[3] (2020) 378-385.
4. L. Deng, L. Ding, K. Zhou, S. Huang, Z. Hu, and B. Yang, J. Magn. Mater. 323[14] (2011) 1895-1898.
5. Y.J. Yang, C.L. Chen, and D.Y. Chen, Magnetochemistry 8 (2022) 75.
6. T.T. Li, Y. Li, R.N. Wu, H. Zhou, X.C. Fang, S.B. Su, A.L. Xia, C.G. Jin, and X.G. Liu, J. Magn. Magn. Mater. 393 (2015) 325-330.
7. V.I. Itin, A.I. Kirdyashkin, and R.V. Minin, Russ. Non-Ferr. Met. 47 (2006) 20-24.
8. G.R. Gordani, M. Mohseni, A. Ghasemi, and S.R. Hosseini, Mater. Res. Bull. 76 (2016) 187-194.
9. J. Tang, D. Li, H. He, Y. Li, J. Zeng, and C. Liu, Appl. Phys. A. 126 (2020) 277.
10. P. Gornert, E. Sinn, and W. Schuppel, IEEE Trans. Electromagn. C. 26 (1990) 12-24.
11. M.J. Iqbal, R.A. Khan, S. Takeda, S. Mizukami, and T. Miyazaki, J. Alloys Compd. 509 (2011) 7618-7624.
12. Z. Su, Y. Chen, B. Hu, A.S. Sokolov, S. Bennett, L. Burns, X. Xing, and V.G. Harris, J. Appl. Phys. 113 (2013) B305.
13. T. Akhter, H.M. Khan, S. Honey, and S.S. Hussain, Ceram. Int. 48 (2022) 33177-33184.
14. X.F. Niu, X.S. Liu, S.J. Feng, and L.V. Farui, J. Ceram. Soc. Jpn. 123 (2015) 920-923.
15. A.L. Ghasemi, Ceram. Int. 42 (2016) 4143-4149.
16. X. Niu, X. Liu, S. Feng, F. Lv, F. Huang, X. Huang, Y. Ma, and K. Huang, J. Optik. 126 (2015) 5513-5516.
17. M.N. Akhtar, K. Ali, A. Umer, T. Ahmad, and M.A. Khan, Mater. Res. Bull. 101 (2018) 48-55.
18. M.J. Iqbal and R.A. Khan, J. Alloys Compd. 478 (2009) 847-852.
19. M.J. Iqbal and S. Farooq, J. Alloys Compd. 505 (2010) 560-567.
20. Y.F. Wu, Y. Huang, and L. Niu, J. Magn. Magn. Mater. 324 (2012) 616-621.
21. J.J. Xu, H.F. Zou, and H.Y. Li, J. Alloys. Compd. 490 (2010) 552-556.
22. I. Khan, M.N. Ashiq, I. Sadiq, A.M. Qureshi, and M.U. Rana, J. Chem. Soc. Pak. 34 (2012) 579-583.
23. M.J. Iqbal, R.A. Khan, S. Mizukami, and T. Miyazaki, Ceram. Int. 38 (2012) 4097-4103.
24. K.Y. Jin and K.S. Soo, IEEE Trans. Magn. 38 (2002) 3108-3110.
25. F. Leccabue, R. Panizzieri, G. Albanese, G. Leo, and N.S. Almodovar, Mater. Res. Bull. 23 (1988) 263-275.
26. A. Goldman, Modern ferrite technology, Springer, 2006.
27. F.K. Lotgering, P.H.G.M. Vromans, and M.A.H. Huyberts, J. Appl. Phys. 51 (1980) 5913-5918.
28. T.R. Wagner, J. Solid State Chem. 136 (1980) 120-124.
29. J. Tang, X.S. Liu, D. Li, and Y.J. Yang, J. Mater. Sci.: Mater. Electron. 30 (2019) 284-291.
30. F.R. Lv, X.S. Liu, and S.J. Feng, Mater. Lett. 157 (2015) 277-280.
31. G. Albanese, M. Carbucicchio, and G. Asti, J. Appl. Phys. 11 (1976) 81-88.
32. S. Ram and J.C. Joubert, J. Magn. Magn. Mater. 99 (1991) 133-144.
33. E.P. Wohlfarth, North-Holland Publishing Company: Amsterdam, The Netherlands 3 (1982) 395-396.
34. I. Khan, I. Sadiq, M.N. Ashiq et al., J. Alloys Compd. 509.31 (2011) 8042-8046.
35. D.Y. Li, F. Wang, A.L. Xia, L.J. Zhang, T.T. Li, C.G. Jin, and X.G. Liu, J. Magn. Magn. Mater. 417 (2016) 355-358.